Pramana – J. Phys. (2019) 93:2
https://doi.org/10.1007/s12043-019-1765-8

Analytical evaluation of cesium emission lines using laser-induced breakdown spectroscopy

MANJEET SINGH[1,2] and ARNAB SARKAR[1,2,*]

[1]Fuel Chemistry Division, Bhabha Atomic Research Centre, Mumbai 400 094, India
[2]Homi Bhabha National Institute, Anushaktinagar, Mumbai 400 094, India
*Corresponding author. E-mail: arnab@barc.gov.in; asarkar@ymail.com

MS received 1 August 2018; revised 27 November 2018; accepted 13 December 2018;
published online 16 April 2019

Abstract. A laser-induced breakdown spectroscopy-based method has been successfully developed to quantify cesium (Cs) in solution using spectroscopically pure graphite planchets as a sample support. As Cs is a line-poor system, only five usable Cs atomic emission lines could be found and characterised by employing high-resolution system. The calibration curves of these emission lines were constructed under optimised experimental conditions. The analytical properties of these calibration curves were evaluated based on the usable dynamic range, R^2 of fitting, root mean square error cross-validation and limit of detection (LOD). The dynamic ranges of these five lines were found to be in correlation with the energy level involved in the transition. An LOD of 4 ppm was obtained using Cs(I) 852.11-nm line, which corresponds to 0.16 μg of Cs on the planchet. Based on the cross-validation approach, the best accuracy and precision ($\sim$6%) were obtained for 852.11 nm in $<$3000 ppm solutions, and the same is $\sim$8% for 672.33 nm and 697.33 nm in high concentrated solution of Cs.

Keywords. Laser-induced breakdown spectroscopy; emission; spectroscopy; cesium; linear dynamic range.

PACS Nos 42.62.Fi; 52.38.Mf; 87.64.K.–; 77.84.Bw; 52.25.Os

1. Introduction

Rapid and accurate identification of fission products, actinides and activated products is the need of the hour in the present age of nuclear energy. Especially in the aftermath of the Fukushima accident, fast and reliable radioactive contamination monitors not only on the premises of nuclear establishments but also in the surrounding areas are required to strengthen emergency preparedness. The earthquake of magnitude 9 and the resultant tsunami that occurred on 11 March 2011 caused damage to the Fukushima Daiichi Nuclear Power Plants (FNPP) to such an extent that it was declared an International Nuclear and Radiological Event Scale (INES) level 7 (out of maximum 7) accident [1]. The event caused large-scale dispersion of radioactive materials in the environment. Among all these materials ^{137}Cs ($t_{1/2}$ = 30.1 years) is of the biggest concern for the next $\sim$300 years (10 half-lives). These dispersed ^{137}Cs would remain radiologically active. Cs is a cation in soil/water and moves upward in the soil profile by plant uptake, thereby having adverse effects on agriculture and thus on human life. Before the incident, Cs concentration near the FNPP site in water was in the sub-parts per billion (sub-ppb) levels, which has increased to several parts per million (ppm) levels after the accident [2]. Inomata *et al* [3] reported that the amount of ^{137}Cs released by the FNPP accident increased the North Pacific ocean's Cs inventory by $\sim$20%. These results prove that vigilant surveillance and monitoring are required to control the ^{137}Cs spread. ^{137}Cs is a radiotoxic element, but if used in a controlled manner, e.g. blood irradiator (^{137}CsCl is used for blood irradiation), it is an asset. Recently, the Bhabha Atomic Research Centre (BARC), India, has developed ^{137}Cs glass pencil by immobilising ^{137}Cs in a glass matrix, which increases its safety during its use in a public domain. Presently, 10% Cs by weight is being loaded in the glass matrix, and studies are going on to increase this loading [4].

In view of their ease and convenience, radiometric methods (β-ray analysis or γ spectroscopy) are employed for the regular analysis of ^{137}Cs. Despite the better sensitivity of radiometric methods, the regularity of their use is limited due to safety, legal

considerations for carrying and storing radioactive samples, and subsequent waste disposal. In high ^{137}Cs-containing sample such as Cs pencil, due to high radioactive doses and radiation self-attenuation, the exact quantification of Cs concentration becomes erroneous using radiometric method.

A better practical and reasonably sensitive alternative in sub-ppm to percentage level is obviously desirable for the determination of Cs. Laser-induced breakdown spectroscopy (LIBS) is a non-contact analysis technique with remote sensing capability. It can work on a stand-alone power system because of its low energy consumption, as demonstrated recently by Curiosity on NASA's Mars mission [5–8]. In addition, the microdestructive nature of LIBS alleviates the problems of storage and disposal of radioactive waste. The International Atomic Energy Agency's (IAEA) technical meeting on Safeguards (2006) emphasised on the need for instrumentation based on LIBS for the positive elemental identification in nuclear fuel cycle processes and associated materials for the nuclear proliferation safeguard purpose.

A good number of studies are reported in the literature for monitoring radioactive and related materials in nuclear industry, such as U, Th, Pu, Sr, B, Li, stainless steel, etc. [9–16]. But reports of Cs using LIBS are limited in number [17–20]. Ikezawa *et al* [18] studied Cs mineral (pollucite) by LIBS using Cs(I) 672.45-nm and Cs(I) 852.11-nm lines in air and predicted the limit of detection (LOD) to be 0.2 ppb based on comparison with a reported Na study using the same methodology. The same group also studied the Cs quantification in soil and sea sand using Cs(I) 672.45 nm [17]. Metzinger *et al* [19] spiked human blood with Cs and obtained an LOD of 6 ppm for Cs(I) 852.11 nm, which was about three orders of magnitude higher than the acceptable level of Cs concentrations (1 ppb) in human blood plasma. Ramli *et al* [20] was able to obtain an LOD of 0.2 ppm of Cs in water using pre-concentration of Cs by electrochemical method and then analysing in 0.5 kPa N_2 ambient gas atmosphere using Cs(I) 852.11-nm line. The reported LOD for Cs in the soil in the same study was 0.3 ppm under low pressure [20]. None of these reported methods were able to detect normal or safe Cs concentrations of 1 ppb in their respective study, but certainly adequate enough at elevated concentrations, under nuclear fallout conditions. To the best of our knowledge, there are no reported studies that have evaluated the properties of all the Cs emission lines except the aforementioned two lines with respect to a calibration curve. The usefulness of these emission lines in different concentration dynamic ranges, especially in the percentage level found in Cs pencil, is also absent in the literature.

The main objective of this study is the real-time monitoring of non-radioactive ^{133}Cs contamination of water through LIBS. All the detectable Cs emission lines, their linear dynamic ranges and LODs will be discussed in this paper. The optimum experimental conditions and detection features, comparisons with literature reports, will also be discussed in this paper.

2. Experimental details

2.1 *Experimental set-up*

A common configuration for a laboratory LIBS system was used for this study. A 532-nm Nd:YAG laser (Brilliant B, Quantel, 5 ns, 10 Hz) was focussed using a plano-convex lens ($f = 10$ cm) to produce a microplasma on the sample surface in an ambient air atmosphere. A previous study by our group has shown that with increasing laser frequency, accuracy–precision of LIBS method also increases [21]. Based on this knowledge, initially 266 nm was chosen for the study, but due to high instability of laser energy at 266 nm, the next available low frequency, the second harmonic 532 nm, was finalised. The distance between the sample and focussing lens was set at 9.8 cm to avoid air breakdown before sample ablation. A collimator equipped with an off-axis parabolic mirror and a meniscus lens was used for collecting light. The collimator images the plasma emissions on to an optical fibre of 200 μm core diameter and is transported through the fibre and finally imaged in front of the entrance slit (40 μm width) of a 750-mm focal length Czerny–Turner spectrometer (Shamrock SR750, Andor, UK). A resolution of 55 pm full-width at half-maximum (FWHM) could be achieved simultaneously over a spectral range of 14 nm using holographic 1800 lines/mm grating. The spectral window for recording is moved stepwise by rotating the grating on its axis via a stepping motor controlled by the software (Solis 4.28). This enables spectral recording over the 200–900 nm wavelength range. An ICCD camera (iStar, Andor, UK, 1024 $\times$ 1024 pixels) embedded with delay generator was used for the detection of emission lines. The quantum efficiency (QE) of the detector varies from 18% at 450 nm to 2% at 800 nm. This detection system allowed spectra to be recorded at suitable acquisition time delay (t_d) and gate width (t_g). The wavelength and efficiency calibrations of the spectrograph–ICCD were carried out using NIST-certified deuterium–quartz–tungsten–halogen (DH2000, Ocean Optics, USA) and Hg–Ar lamps (HG-1, Ocean Optics, USA), respectively. A pyroelectric energy meter with a high damage threshold diffuser along with a handheld power meter (Ophire

Photonics, Israel) was used for measuring the energy of the laser pulse. The samples under investigation were placed on a micrometre-driven *XYZ* translation platform (M/s Velmex, Inc., USA). All possible displacements to optimise the sample position were remotely controlled through an in-house written LabVIEW-based program. Graphite furnace atomic absorption spectrometry (GFAAS) analysis was carried out using ZEEnit 650 spectrometer (M/s Analytik Jena, Germany). For GFAAS analysis, 582.1 nm wavelength with 7 mA lamp current was used. SSG grade 1 argon (99.999%), with 3 l/min flow rate, was used as a protective and purge gas.

2.2 *Sample preparation*

Due to the unavailability of commercially available Cs calibration solution with the author, calibration solutions of Cs were prepared in the laboratory using supra-pure cesium chloride (≥99.995%, M/s Merck Life Science Private Limited, India). Initially, a stock solution of 10,000 ppm of Cs was prepared by dissolving accurately weighted CsCl in supra-pure grade concentrated HNO_3. The solution was then evaporated to dryness, and the residues were re-dissolved in 1 M HNO_3. Suitable dilutions were then made from this stock solution to prepare calibration solutions of 2–7000 ppm concentration range as shown in table 1. As the anhydrous CsCl is unsuitable for accurate weighing, the prepared solutions needed concentration standardisation, which was done by analysing the solutions by GFAAS. The concentration data determined by GFAAS have an accuracy of ±5% (table 1).

Table 1. Cs calibration solution concentration determined by GFAAS having 5% error along with the corresponding amount of Cs in 40 μl solution.

Sample No.	GFAAS concentration of Cs (ppm)	Amount of Cs in 40 μl (μg)
C10000	10059 ± 503	402 ± 20
C7000	7027 ± 351	281 ± 14
C5000	5055 ± 253	202 ± 10
C3000	2997 ± 150	120 ± 6
C1000	985 ± 49	39 ± 2
C700	666 ± 33	27 ± 1
C500	472 ± 24	18.9 ± 0.9
C300	305 ± 15	12.2 ± 0.6
C100	115 ± 6	4.6 ± 0.2
C70	78 ± 4	3.1 ± 0.2
C50	58 ± 3	2.3 ± 0.1
C25	29 ± 1.5	1.2 ± 0.06
C10	12 ± 0.6	0.5 ± 0.03
C5	6 ± 0.3	0.2 ± 0.01
C1	2 ± 0.1	0.1 ± 0.01

2.3 *LIBS analysis*

For the analysis of a liquid sample by LIBS, solid substrate support methodology developed by Sarkar *et al* [9,12] was used. Cs solution of 40 μl was transferred drop-wise through a volumetric pipette (Eppendorf, Germany), on to a graphite planchet (M/s Ted Pella, Inc., USA) of 32 mm diameter and 1.6 mm width. High-purity graphite planchets were used in the study to avoid any spectral interference at the line of interest by any impurity emission lines. The solution was then evaporated to dryness under IR lamp to create a dried spot of ∼10 mm diameter on the planchet. Subsequently, the planchet was allowed to cool to room temperature and was then mounted in the sample chamber for analysis. Effectively, only a few tens of micrograms of Cs were loaded on the graphite planchet as shown in table 1. Triplicate analyses were carried out for each sample, under identical experimental conditions. Initially, the C1000 sample was analysed for selection of emission lines in 200- to 900-nm region. Thereafter, only the required region was analysed. The diameter of the crater formed due to laser ablation was found to be about 150 μm, which was measured using an optical microscope equipped with 25× objective lens. To avoid any cross-contamination due to ablation, the subsequent laser spot was focussed 200 μm apart in the *xy*-plane by controlling the translational stage. The dried spots will not have uniform Cs distribution due to coffee-spot effect. Hence, to record the LIBS spectra, 12-mm line scan along the diameter of the spot was done. This resulted in the accumulation of 60 single-shot LIBS spectra, each on a fresh surface for one spectrum recording.

An in-house written program in LabVIEW, to fit the peaks in the Lorentzian profile, was used to calibrate Cs LIBS spectra. The Lorentzian peak area along with the Cs calibration concentration was used to construct a calibration curve model based on linear regression analysis. The analytical properties of these calibration models were evaluated based on a linear dynamic range, R^2 of fitting (the closer to 1, the better the fit), root mean square error cross-validation ($RMSE_{cv}$; smaller the $RMSE_{cv}$, the better the fit) and LOD:

$$R^2 = 1 - \left(\sum_{i=1}^{i}\sum_{j=1}^{j}\left(C_s^i - C_j^i\right)^2\right) \Big/ \left(\sum_{i=1}^{i}\left(C_s^i - \frac{1}{i}\sum_{i=1}^{i}C_s^i\right)^2\right), \quad (1)$$

$$\mathrm{RMSE_{cv}} = \sqrt{\left(\sum_{i=1}^{i}\sum_{j=1}^{j}\left(C_{\mathrm{s}}^{i} - C_{j}^{i}\right)^{2}\right)\Big/\mathrm{DOF}}, \quad (2)$$

$$\mathrm{LOD} = (3\sigma/m) + C_{\mathrm{s}}^{i=0}. \quad (3)$$

Here, i represents the total number of samples used for the particular calibration model and j is the number of replicate analyses, which is 3 in the present case. C_j^i is the predicted concentration of the jth replicate of the ith sample by calibration model. C_{s}^i is the calibration concentration of the ith sample tabulated in table 1. DOF is the degree of freedom. σ is the standard deviation of the background or of the sample signal obtained from the sample with the lowest concentration in the used dynamic range ($C_{\mathrm{s}}^{i=0}$) and m is the slope of the calibration curve.

The analytical predictive property of a calibration model is evaluated based on relative cross-validation accuracy (%$\mathrm{RA_{cv}}$) and relative standard deviation of cross-validation (%$\mathrm{RSD_{cv}}$):

$$\%\mathrm{RA_{cv}} = \frac{100}{i_{\max}-2} \times \sum_{i=2}^{i_{\max}-1}\left\{\left(\sum_{j=1}^{j}\left|C_j^i - C_{\mathrm{m}}^i\right|\Big/C_{\mathrm{m}}^i\right)\Big/ j_{\max}\right\}, \quad (4)$$

$$\%\mathrm{RSD_{cv}} = \frac{100}{i_{\max}-2} \times \sum_{i=2}^{i_{\max}-1}\left\{\sqrt{\sum_{j=1}^{j}(C_j^i - C_{\mathrm{m}}^i)^2/(j_{\max}-1)}\Big/C_{\mathrm{m}}^i\right\}. \quad (5)$$

Here, C_{m}^i is the mean predicted concentration of the ith sample. To eliminate any arbitrary result at the end of dynamic range, which is usually obtained in the cross-validation study, the first and the last samples of a particular dynamic range were not used for the calculation of the above statistical data. Leave-one-out cross-validation method was used in this study.

3. Results and discussions

3.1 *Condition optimisation*

A spectrally interfered emission line generates a calibration model of degraded quality. Hence the selection of proper emission lines is an important criterion for the development of calibration models. LIBS spectra of the C1000 sample were recorded from 200 up to 900 nm. After analysing these spectra and correlating with the literature survey [17–20], NIST database [22] and Kurucz database [23], seven Cs emission lines were identified and selected (table 2). Figure 1 shows the seven emission lines identified in the C1000 sample analysed at a laser energy of 50 mJ and t_{d} of 2 μs. The emission intensity of the two emission lines, Cs(I) (698.35 nm) and Cs(I) (894.35 nm), was too low compared to the other Cs emission lines and hence was not used further for any calibration-related study. The low intensity of Cs(I) (698.35 nm) compared to Cs(I) (697.33 nm) is due to the low transition probability, but for Cs(I) (894.35 nm), the low QE of the ICCD is the probable reason. Using a high QE detector in the 890-nm region may be helpful to study the Cs(I) (894.35 nm) emission line.

The sensitivity of the LIBS measurements depends on many factors: the light collection angle (t_{g}), laser energy (t_{d}), the nature of the analyte, laser wavelength (E_{L}), sensitivity of the optical set-up, etc. Among these parameters, the three most important parameters pertain to the role played by E_{L}, t_{d} and t_{g}, and this aspect has been discussed in detail in many literatures [24–26]. t_{g} was fixed at 50 μs which virtually covers the whole plasma lifetime, thereby increases the signal. The signal-to-background ratio (SBR) and the signal-to-noise ratio (SNR) are important parameters for comparing the signal quality. The noise is calculated as one standard deviation (1σ) of the background signal's variation, which is calculated using the adjacent area of the peak of interest. In this study, it was observed that the degree of noises was negligible in the spectra obtained in any experimental conditions. This characteristic of SNR makes it unsuitable for optimisation study. Hence, the SBR data were monitored for optimisation of E_{L} and t_{d} parameters. All the seven selected Cs(I) emission lines were used for carrying out the optimisation study. For the optimisation experiments, the line intensity must be sufficiently high to be observed in high t_{d} and also must not get self-saturated in high E_{L}. Considering these two factors, C1000 sample was chosen for the optimisation analysis. The SBR was measured by varying t_{d} at a particular E_{L} value. Figure 2 shows a typical contour diagram of SBR for E_{L} vs. t_{d} obtained using Cs(I) (852.11 nm) emission line originating from Cs1000 sample. It is seen that in the range $1.5 < t_{\mathrm{d}} < 2.5$ μs and $45 < E_{\mathrm{L}} < 65$ mJ, the SBR for Cs(I) 852.11 nm was the highest. Other emission lines also showed similar range and hence, E_{L} of 55 mJ and t_{d} of 2 μs were chosen as optimum analysis conditions for Cs analysis in this study.

Table 2. Characteristics of Cs emission lines employed for LIBS analysis.

Cs(I) wavelength (nm)	Transition coefficient (A_{ij}) (s^{-1})	Lower energy level (E_j) (cm^{-1})	Upper energy level (E_i) (cm^{-1})	References
455.53	1.84×10^6	0	21946.397	[23]
459.32	7.94×10^5	0	21765.348	[23]
672.33	5.27×10^6	11178.270	26047.860	[22]
697.33	7.51×10^6	11732.308	26068.830	[22]
698.35	1.29×10^6	11732.308	26047.860	[22]
852.11	3.28×10^7	0	11732.307	[23]

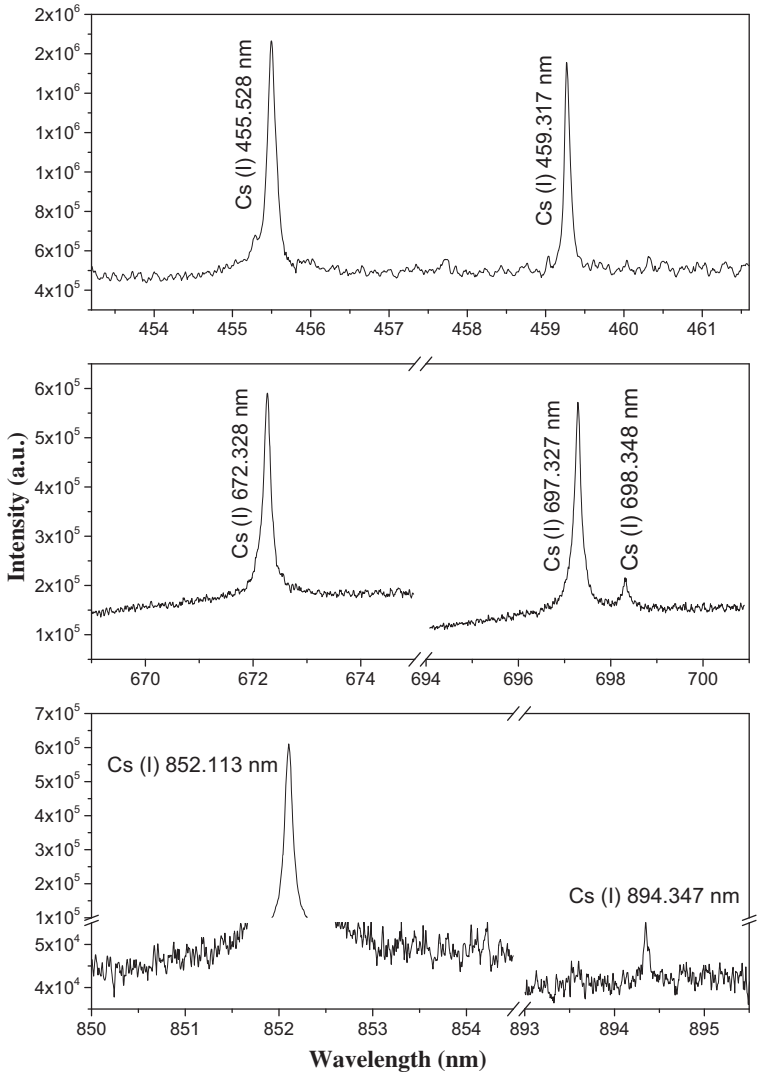

Figure 1. Accumulation of 60 single-shot LIBS spectra of Cs solution on a graphite planchet at a laser energy of 50 mJ and acquisition delay of 2 μs.

3.2 *Calibration curves*

The spectral line profile is determined by the dominant broadening mechanism involved in the evaluation of the peak. Among three main broadening mechanisms involved in a laser-induced plasma evaluation, Doppler broadening results in a Gaussian profile, whereas the natural line broadening and collision broadening lead to a Lorentz profile. When the Doppler and collision broadening are of comparable magnitudes, the Voigt function (convolution of Gaussian and Lorentz profiles) might be preferred to fit peaks accurately.

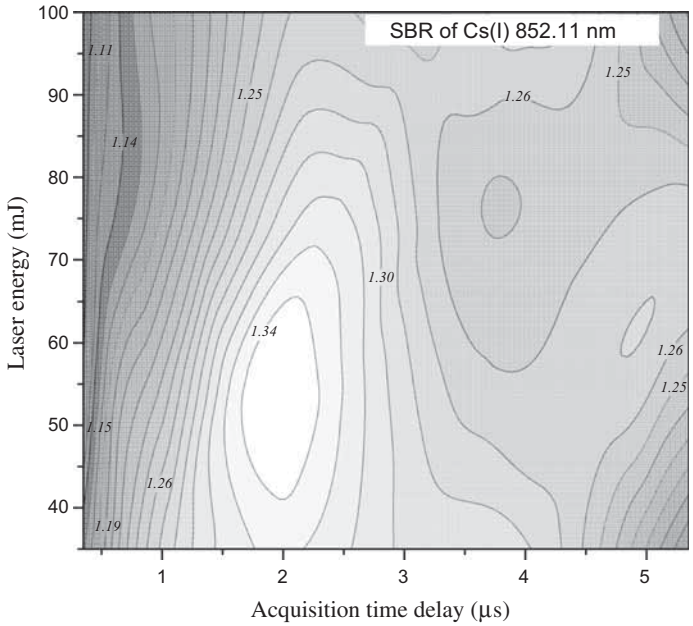

Figure 2. Contour diagrams of Cs(I) (852.11 nm) emission line showing the effects of t_d and E_L on the SBR.

However, in LIBS plasma, the collision broadening dominates over Doppler, and hence, the spectral lines were fitted with the Lorentz function [27]. Calibration curves were constructed by plotting the Lorentzian peak fitted area against the GFAAS concentration of Cs.

Figure 3 shows the intensity of peak plotted against the concentration of Cs solution. The vertical line shows the error ($\pm 1\sigma$) on triplicate analysis. It can be seen from figure 3 that none of the five emission lines have a universal linear response range. For all the emission lines, there exist lower and upper concentration limits, between which the response of LIBS signal strength is linearly dependent on the solution's Cs concentration. This range is known as a linear dynamic range of the respective calibration curve under the experimental conditions. In this study, the difference between the two adjacent concentrations of solutions was kept large to cover wider concentration range. Hence, the obtained values of lower and upper limits of a dynamic range are not rigid and must be considered with an error of 10% (table 3).

Apart from Cs(I) (672.33 nm) and Cs(I) (697.33 nm), other three emission lines were found to show signal strength and t_d non-linearity in the high concentration region. For Cs(I) (672.33 nm) and Cs(I) (697.33 nm), linearity was observed up to ∼10000 ppm (highest concentration in this study), which correspond to 402 μg of Cs deposition on ∼0.8 cm^2 area on the surface of the graphite planchet. The deviation from linearity in a calibration curve at high concentrations is most often due to the self-absorption phenomenon. Self-absorption is more prominent in resonance line emission lines, i.e. emission line with the lower level of the transition is the ground state. In a LIBS plasma, the outer layer is populated mostly with atoms in the ground state (cool atoms), whereas the centre of the plasma contains hot atoms (excited state). As the hot atoms decay and emit photons, the cooler atoms at the outer layer reabsorb the resonance photon, thus reduce the recorded intensity of the emission line. As the concentration of the atoms in the target sample increases, the self-absorption becomes more and more evident. Cs(I) (672.33 nm) and Cs(I) (697.33 nm) are non-resonant lines, and hence are less prone to self-saturation [28–30]. Cs(I) (455.53 nm) and Cs(I) (459.32 nm) show self-saturation effect above ∼5000 ppm concentration in this study and the same for Cs(I) (852.11 nm) starting above ∼3000 ppm concentration. This trend is expected as these three lines are resonant emission lines. The early starting of self-saturation with respect to the concentration for Cs(I) (852.11 nm) is due to 10 times higher transition probability of Cs(I) (852.11 nm) than Cs(I) (455.53 nm) and Cs(I) (459.32 nm), leading to the onset of self-saturation at a lower concentration region.

For the two non-resonant emissions, Cs(I) (672.33 nm) and Cs(I) (697.33 nm), the high excitation level along with relatively low transition probability causes the emission lines to be strong enough for detection only after certain high concentration (∼1000 ppm) which is the lower limit of the linear dynamic range [22]. Cs(I) (852.11 nm) has the lowest upper energy level among the

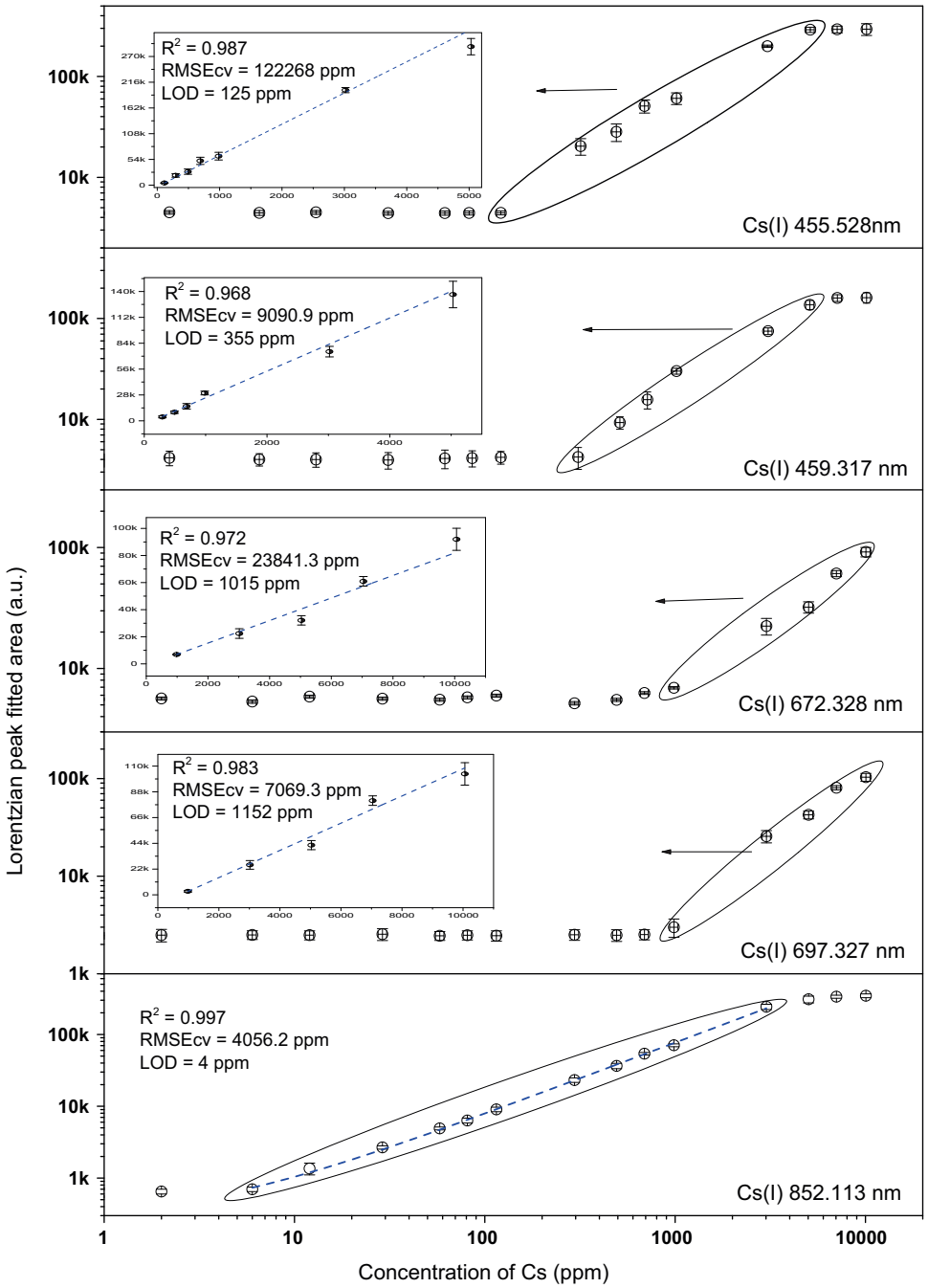

Figure 3. Dynamic range and the constructed calibration curves in the respective dynamic range for the Cs(I) (455.53 nm), Cs(I) (459.33 nm), Cs(I) (672.33 nm), Cs(I) (697.33 nm) and Cs(I) (852.11 nm).

five emission lines and also high transition probability making it sensitive up to a few ppm concentration levels. For Cs(I) (455.53 nm) and Cs(I) (459.32 nm), the upper energy level is almost the same, but relatively smaller transition probability of Cs(I) (459.32 nm) causes the lower limit of a dynamic range to be higher (∼300 ppm) than that of Cs(I) (455.53 nm) (∼100 ppm).

Linear calibration curves were constructed using the selected dynamic ranges. The calibration properties of the constructed calibration curves are also tabulated in table 3. Cs(I) (852.11 nm) shows the highest sensitivity (highest slope) as stated above. The two other resonant lines, Cs(I) (455.53 nm) and Cs(I) (459.32 nm), show moderate sensitivity. The two non-resonant emission lines, Cs(I) (672.33 nm) and Cs(I) (697.33 nm), show the lowest sensitivity having a slope of 16.6 and 11.5, respectively. Although $RMSE_{cv}$ is a good parameter for comparing the error of the constructed calibration

Table 3. The calibration properties along with the analytical predictive properties of the Cs emission line calibration models.

Cs(I) emission line (nm)	Dynamic range (ppm) (±5%)	Slope	Intercept	R^2	$RMSE_{cv}$ (ppm)	LOD		$\%RA_{cv}$	$\%RSD_{cv}$
						ppm	μg		
455.53	100–5000	58.7	5435.2	0.987	12226.8	125	5	10.65	9.48
459.32	300–5000	26.2	−1857.2	0.968	9090.9	355	14	10.28	9.94
672.33	1000–10000	16.6	−28858	0.972	23841.3	1015	41	8.08	7.93
697.33	1000–10000	11.5	−8910.7	0.983	7069.3	1152	46	7.35	7.51
852.11	6–3000	82.5	−1738.9	0.997	4056.2	4	0.16	5.89	5.28

curves, due to the different dynamic ranges and thus the number of standards, direct comparison of this value will lead to wrong conclusion. The emission lines with the same dynamic range, i.e. Cs(I) (672.33 nm) and Cs(I) (697.33 nm) can be compared and $RMSE_{cv}$ of these two lines indicate that Cs(I) (697.33 nm) has superior calibration properties than Cs(I) (672.33 nm). The LODs of these emission lines are calculated using eq. (3) and are shown in table 3. The best LOD is obtained for Cs(I) (852.11 nm), which is 4 ppm, owing to its high slope and low lower limit of the dynamic range. In terms of LOD, the other emission lines are of poor quality. The LODs range from 100 s of ppm to 1000 s of ppm. The poor LODs are due to the very low sensitivity of the emission lines in the low concentration dynamic range. However, the amount of Cs deposited on the graphite planchet is in submicrograms to a few tens of micrograms, indicating a very good sensitivity of the present LIBS study.

This study employed a conventional LIBS approach for Cs quantification. The obtained results are comparable with the results obtained by Metzinger *et al* [19] employing a very similar approach by drying the liquid samples on a metallic plate to obtain a Cs LOD of 6 ppm in urine sample and 27 ppm in blood sample. But the results are far superior to the LODs shown by Ikezawa *et al* of around 1000 ppm in sand samples using conventional direct sample analysis method [17]. Only the results shown by Ramali *et al* [20] have better LOD than this study using sophisticated methodologies. Ramali *et al* [20] showed that the LODs can be reduced to 0.3 ppm in sand and 0.2 ppm in water using low-pressure N_2 atmosphere.

The analytical predictive property of a calibration model is best judged by comparing the accuracy and precision of the analysis and not only the LOD. The prediction quality in this study was measured by determining the $\%RA_{cv}$ and $\%RSD_{cv}$ values (table 3). Cs(I) (852.11 nm) shows an accuracy–precision of 5–6%. Cs(I) (852.11 nm) also has the least LOD among the five emission lines. The two non-resonant lines show an accuracy–precision of 7–8% which is marginally poorer than the calibration quality of Cs(I) (852.11 nm). Relatively worse performance with respect to accuracy and precision was obtained for the two resonance emission lines, Cs(I) (455.53 nm) and Cs(I) (459.32 nm). Both the accuracy and precision for these two lines are ∼10%.

4. Conclusions

Cs atomic emission line calibrations were compared qualitatively and quantitatively using the spectra obtained from a Cs aqueous solution deposited on a graphite planchet. Five Cs(I) emission lines (455.53, 459.32, 672.33, 697.33 and 852.11 nm) were used to develop the calibration models. The quality of these calibration models was evaluated based on the dynamic range, R^2 of fitting, $RMSE_{cv}$ and LOD. The dynamic ranges of these five lines are very much different. The two non-resonant lines, Cs(I) (672.33 nm) and Cs(I) (697.33 nm), are only useful in the high concentration range (1000–10000 ppm), whereas the resonant lines Cs(I) (852.11 nm) is sensitive in the low dynamic range (<3000 ppm). These calibration models were used to predict the Cs concentration based on the cross-validation principle. Based on the result of $\%RA_{cv}$ and $\%RSD_{cv}$, Cs(I) (455.53 nm) and Cs(I) (459.32 nm) are found to be the poorest with respect to accuracy and precision (10%). The best prediction quality (∼6%) was shown by Cs(I) (852.11 nm) but it fails above the 3000 ppm concentration due to the self-saturation effect. Cs(I) (672.33 nm) and Cs(I) (697.33 nm) exhibited ∼8% accuracy and precision and can be used in the high concentration range only. The values of LODs obtained using Cs(I) (852.11 nm) lines have lower (better) values than those from the other atomic lines with the best LOD of 4 ppm, which correspond to 0.16 μg of Cs on the planchet. The results clearly demonstrate the applicability of the LIBS for monitoring the environment contamination in the case of an unwanted disaster causing a high level of Cs contamination, like the Fukushima accident. Again, in the case of very high level of Cs, such as in Cs

blood irradiator pencil, Cs(I) (672.33 nm) and Cs(I) (697.33 nm) will be useful for quantification as they will not show self-saturation. The developed method also provides an independent approach based on different physicochemical principles for the determination of Cs.

Acknowledgements

The authors acknowledge Dr. P G Jaison, Head, Mass Spectrometry Section and Dr. S Kannan, Head, Fuel Chemistry Division, BARC, for their constant support and encouragement in LIBS work. This work was funded by the BARC, DAE.

References

[1] J Lelieveld, D Kunkel and M G Lawrence, *Atmos. Chem. Phys.* **12**(**9**), 4245 (2012)
[2] T J Yasunari, A Stohl, R S Hayano, J F Burkhart, S Eckhardt and T Yasunari, *Proc. Natl. Acad. Sci.* **108**(**49**), 19530 (2011)
[3] Y Inomata, M Aoyama, T Tsubono, D Tsumune and K Hirose, *Environ. Sci.: Process. Impacts* **18**(**1**), 126 (2016)
[4] C P Kaushik, A Kumar, N S Tomar, S Wadhwa, D Mehta, R K Mishra, Jyoti Diwan, S Babu, S K Marathe, A P Jakhete, S Jain, G Anand and K Agarwal, Brief Communication, BARC Newsletter Report No. 356 (2017)
[5] N L Lanza, S M Clegg, R C Wiens, R E McInroy, H E Newsom and M D Deans, *Appl. Opt.* **51**(**7**), B74 (2012)
[6] N L Lanza, R C Wiens, S M Clegg, A M Ollila, S D Humphries, H E Newsom and J E Barefield, *Appl. Opt.* **49**(**13**), C211 (2010)
[7] A M Ollila, J Lasue, H E Newsom, R A Multari, R C Wiens and S M Clegg, *Appl. Opt.* **51**(**7**), B130 (2012)
[8] R C Wiens, S Maurice, J Lasue, O Forni, R B Anderson, S Clegg, S Bender, D Blaney, B L Barraclough, A Cousin, L Deflores, D Delapp, M D Dyar, C Fabre, O Gasnault, N Lanza, J Mazoyer, N Melikechi, P Y Meslin, H Newsom, A Ollila, R Perez, R L Tokar and D Vaniman, *Spectrochim. Acta B* **82**, 1 (2013)
[9] A Sarkar, S K Aggarwal, K Sasibhusan and D Alamelu, *Microchim. Acta* **168**(**1–2**), 65 (2010)
[10] A Sarkar, D Alamelu and S K Aggarwal, *Talanta* **78**(**3**), 800 (2009)
[11] A Sarkar, D Alamelu and S K Aggarwal, *J. Nucl. Mater.* **384**(**2**), 158 (2009)
[12] A Sarkar, D Alamelu and S K Aggarwal, *Appl. Opt.* **47**(**31**), G58 (2008)
[13] D A Cremers, A Beddingfield, R Smithwick, R C Chinni, C R Jones, B Beardsley and L Karch, *Appl. Spectrosc.* **66**(**3**), 250 (2012)
[14] P Fichet, P Mauchien and C Moulin, *Appl. Spectrosc.* **53**(**9**), 1111 (1999)
[15] A M Popov, A N Drozdova, S M Zaytsev, D I Biryukova, N B Zorov and T A Labutin, *J. Anal. At. Spectrom.* **31**(**5**), 1123 (2016)
[16] V Karki, A Sarkar, M Singh, G S Maurya, R Kumar, A K Rai and S K Aggarwal, *Pramana – J. Phys.* **86(6)**, 1313 (2016)
[17] S Ikezawa, T Ueda, A Mason, O Korostynska and A Al-Shamma'a, *Proceedings of the International Conference on Sensing Technology, ICST* (2013) (unpublished)
[18] S Ikezawa, M Wakamatsu and T Ueda, *Solid State Phenom.* **199**, 285 (2013)
[19] A Metzinger, E Kovács-Széles, I Almási and G Galbács, *Appl. Spectrosc.* **68**(**7**), 789 (2015)
[20] M Ramli, A Khumaeni, K H Kurniawan, M O Tjia and K Kagawa, *Spectrochim. Acta B* **132**, 8 (2017)
[21] M Singh, A Sarkar, X Mao and R E Russo, *J. Nucl. Mater.* **484**, 135 (2017)
[22] R L Kurucz, Kurucz Atomic Database, http://www.cfa.harvard.edu/amdata/ampdata/kurucz23/sekur.html (23 Oct. 2018)
[23] NIST, in NIST atomic spectral database, http://physics.nist.gov/cgi-bin/ASD/lines_form.html (23 Oct. 2018)
[24] M Kuzuya, H Matsumoto, H Takechi and O Mikami, *Appl. Spectrosc.* **47**(**10**), 1659 (1993)
[25] B Sallé, D A Cremers, S Maurice and R C Wiens, *Spectrochim. Acta B* **60**(**4**), 479 (2005)
[26] B C Castle, K Talabardon, B W Smith and J D Winefordner, *Appl. Spectrosc.* **52**(**5**), 649 (1998)
[27] D A Cremers and L J Radziemski, Basics of LIBS plasma, in *Handbook of laser-induced breakdown spectroscopy* (John Wiley & Sons Ltd, UK, 2006) p. 23
[28] J Hou, L Zhang, W Yin, S Yao, Y Zhao, W Ma, L Dong, L Xiao and S Jia, *Opt. Express* **25**(**19**), 23024 (2017)
[29] J-M Li, L-B Guo, C-M Li, N Zhao, X-Y Yang, Z-Q Hao, X-Y Li, X-Y Zeng and Y-F Lu, *Opt. Lett.* **40**(**22**), 5224 (2015)
[30] D A Cremers and L J Radziemski, LIBS analytical figures of merit and calibration. in *Handbook of laser-induced breakdown spectroscopy* (John Wiley & Sons Ltd, UK, 2013) p. 123